

SURVIVABILITY OF METALLIC SHIELDS

for Relativistic Spacecraft

JON DROBNY¹, ALEXANDER N. COHEN², DAVIDE CURRELI¹, PHILIP LUBIN², MARIA G. PELIZZO³ & MAXIM UMANSKY⁴

¹Department of Nuclear, Plasma, and Radiological Engineering, University of Illinois at Urbana Champaign, Urbana, IL, 61801, USA; ²Department of Physics, University of California - Santa Barbara, Santa Barbara, CA, 93106, USA; ³Consiglio Nazionale delle Ricerche - Istituto di Fotonica e Nanotecnologie (CNR-IFN), 35131 Padova, Italy; ⁴Lawrence Livermore National Laboratory, Livermore, CA, 94550, USA

Email: drobny2@illinois.edu

Directed energy propulsion of a spacecraft, such as that proposed by Breakthrough Starshot and NASA Starlight, necessarily exposes the spacecraft to MeV-energy collisions with particles in the interstellar medium (ISM). As a result, the spacecraft must be designed to be resilient to those collisions and the damaging effects they can have over long-duration interstellar missions. In this work, the effect of cumulative ISM gas implantation along the leading edge cross section of a standard relativistic spacecraft is discussed. Expected effects include bubble formation, blistering, and exfoliation due to slowly diffusing gas atoms implanted deep below the surface. As predicted by Bethe-Bloch stopping and numerical binary collision approximation (BCA) simulations, hydrogen and helium implant at similar depths, producing a mixed hydrogen-helium-material system similar to those observed in plasma-facing components (PFCs) in fusion reactors. A model of the stress exerted by the local gas concentration below the surface of a thin spacecraft and mission failure scenarios which require mitigation strategies are presented.

Keywords: Interstellar, Spacecraft, Damage, Implantation, ISM, Starlight, Starshot

1 INTRODUCTION

In baseline mission proposals [27][25][45], a gram-scale spacecraft is accelerated via a directed energy system to 0.05–0.2c. The spacecraft is composed of a thin, circular semiconductor wafer with a nominal diameter of ~100 mm and thickness ~100 μm. Around the circumference of the spacecraft will be a shield to protect sensitive components from direct exposure to the interstellar medium. An illustration of this spacecraft design and an artist's rendering of the mission profile are shown in Fig. 1. For the analyses in this paper, this spacecraft design is adopted as a standard target for ISM impacts.

1.1 The Local Interstellar Medium (LISM)

The LISM is composed of roughly 99% gaseous matter and 1% granular dust by mass. The gaseous matter is composed of approximately 70% hydrogen and 28% helium by mass, while the remaining 2% is composed of trace amounts of heavier elements, including carbon, oxygen, and iron [13][24]. According to work done by Hoang et al., damage by heavy atoms is limited to track formation to depths of ~0.1 mm [22]. Interstellar dust is composed largely of hydrocarbons, silicates, and ices in the form of grains with characteristic size ~1 μm [13]. Impacts with many small dust grains or single large dust grains may

cause the destruction of relativistic spacecraft, but the estimated probability of total spacecraft destruction is low [22].

On large scales (~10 to 100 ly), the ISM is inhomogeneous and can vary greatly in density. While the majority of the ISM by volume is composed of ionized hydrogen with a density of approximately 1 cm⁻³, common measurements of LIC densities, such as those performed by Gloeckler and Geiss, report combined H and He densities as low as ~0.26 cm⁻³ [18].

From Figure 2, it can be seen that for local stars within 50 ly, the hydrogen column density falls in the range

$$10^{17.5} \leq N_{\text{HI}} \leq 10^{18.3} \text{ cm}^{-2} \quad (1)$$

which is numerically equivalent to the total hydrogen fluence, or dose, Φ_H, incident on a spacecraft travelling along that line-of-sight upon arrival at the target star [38][37].

1.2 Damage to Interstellar Spacecraft by Light Ion Impacts

At speeds relevant to an interstellar mission, 0.05–0.2c, the ISM in the reference frame of a spacecraft appears as a constant-velocity, MeV beam composed primarily of hydrogen and helium that spans the entire front-facing cross section of the spacecraft. At MeV energies, ISM particles impacting the spacecraft will be immediately stripped of their electrons. To investigate the effect of damage by gas accumulation during interstellar flight, the ISM can be treated as a fully ionized, spacecraft-spanning wide beam of hydrogen and helium.

This paper was first presented 6th Interstellar Symposium and NASA Interstellar Propulsion Workshop (formerly formerly the Tennessee Valley Interstellar Workshop), Wichita, USA 10-15 November, 2019.

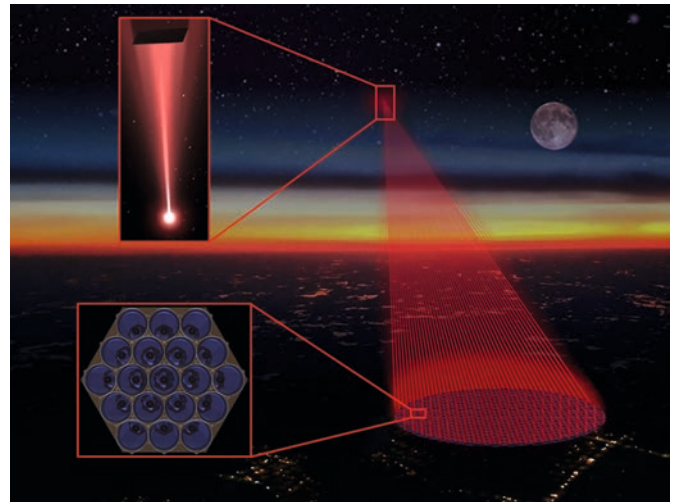
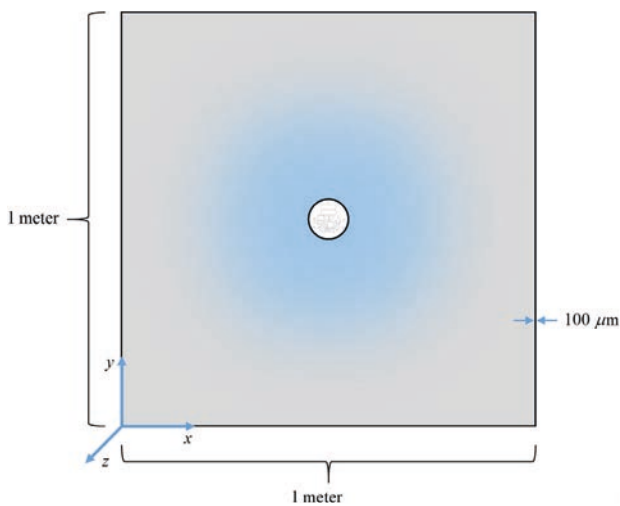


Fig.1 (a) An illustration of a typical Starshot-style spacecraft design. (b) An artist's rendering of a typical Starshot-style mission profile, including the phased laser array for directed propulsion and the spacecraft and solar sail (inset).

Damage caused by heavy ion impacts and dust grain impacts on relativistic spacecraft has been investigated [22]. Therefore, this work will focus on the cumulative effect of light ion interactions with spacecraft shields.

Modeling of ion-solid interactions is commonly done with Binary Collision Approximation (BCA) codes, such as TRIM, TRIDYN, and MARLOWE [4][14][40]. Used here,

SRIM is a free-use Monte Carlo, BCA implementation of TRIM that has been in continuous development since 1985 [53][54]. SRIM includes models of nuclear and electronic stopping valid for energies below the sputtering threshold (10s–100s of eV) through the GeV range for light ions [52], and produces detailed information about ion-solid interactions, including reflection coefficients, sputtering yields, vacancy production, implantation distributions, and detailed

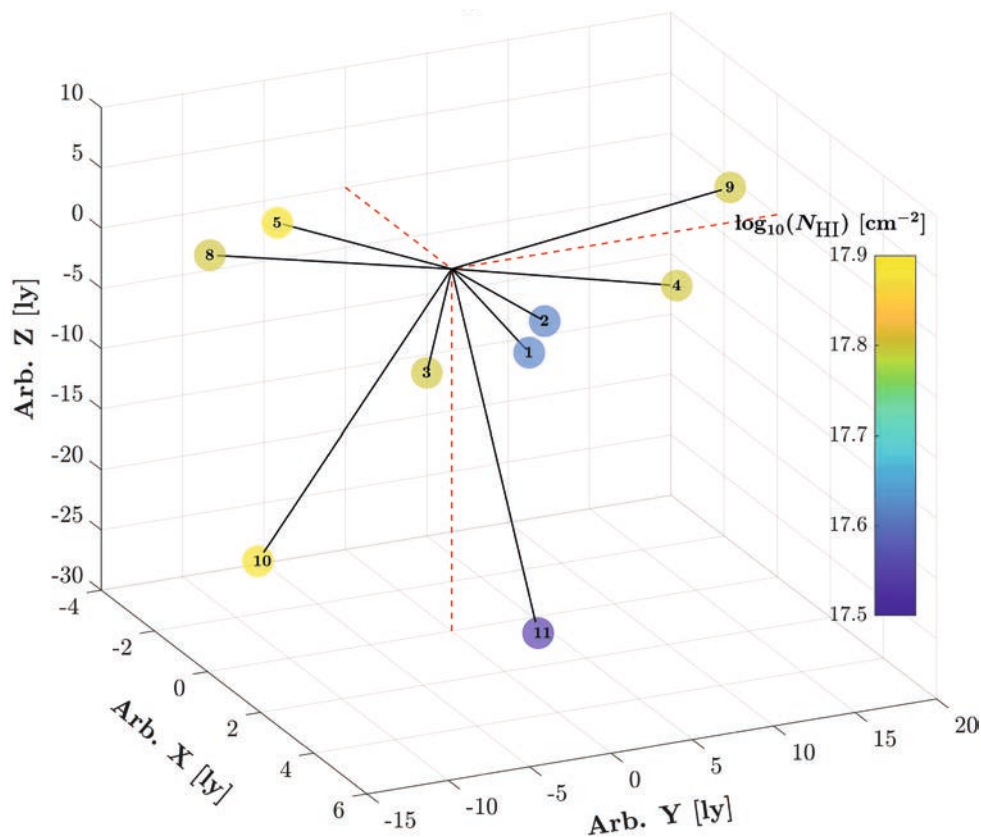


Fig.1 Positions of local stars within ~50 ly from the Sun. The origins of all lines-of-sight vectors correspond to the location of the Sun. The color scale corresponds to the atomic hydrogen column density along the line-of-sight to each star. Data reproduced from [38][37]. The names and characteristics of the stars numbered above are listed in Table 9 in the Appendix.

trajectory information of collision cascade.

To prevent high energy hydrogen and helium from damaging spacecraft components and instruments, it will be necessary to shield the front-facing cross-section of the spacecraft. Metallic shields, due to their high strength, high density, good thermal conductivity, and relatively low sputtering yields when irradiated with light ions, are a natural choice. Fusion plasma-facing components (PFCs) face a similar irradiation environment to relativistic, interstellar spacecraft travelling through the ISM. Both will be exposed to high-fluence simultaneous hydrogen and helium bombardment and undergo a significant number of radiation-induced defects [7]. In particular, ITER will use metallic plasma-facing components, and the response of these materials to simultaneous hydrogen and helium bombardment has been well studied [34]. Several distinct differences between the fusion environment and an ISM exposed relativistic spacecraft deserve mention. First, the particle flux in the latter case will be significantly lower: 10^8 – 10^9 $\text{cm}^{-2}\text{s}^{-1}$ compared to 10^{20} $\text{cm}^{-2}\text{s}^{-1}$ for a DEMO style divertor [23]. Second, the energy of hydrogen and helium will be in the MeV range, compared to the eV–keV range for a fusion divertor between disruptions. Third, the temperature of an interstellar spacecraft will be relatively low, at or below room temperature (say, 20 °C) compared to 700–1000 °C in a fusion divertor [22]. These differences will influence the nature of damage caused by particle flux to the material, but damage mechanisms such as blistering happen universally at nearly all irradiation energies. Due to their success in resisting the damaging effects of light ion damage in fusion PFCs, metallic shields are considered here to protect interstellar spacecraft.

2 DAMAGE TO INTERSTELLAR SPACECRAFT BY LIGHT ION IMPACTS

2.1 Physical Sputtering by Light Ions

Physical sputtering is a process by which incident energetic ions transfer kinetic energy to material atoms, displacing them from their original positions, and through momentum transfer back to the exposed surface, removing atoms therefrom. An atom displaced directly by irradiation is referred to as a primary knock-on. Primary knock-ons with sufficient energy continue to travel through the material, displacing other material atoms in what is referred to as the collision cascade. If sufficient energy is transferred to atoms in the first few mono-layers to overcome the surface binding energy, they may be removed from the surface of the material. For sputtering from normal incidence irradiation, the sputtering yield in atoms removed per ion decreases sharply with increasing energy beyond the energy of maximum sputtering, which is typically in the 100s to 1000s of keV, depending on the incident ion species and target material [30][6]. At high energies, above approximately 1 MeV/amu, ions interact with materials primarily through electronic stopping, not collisions with material atoms. The cross section for nuclear stopping, and thus the likelihood of transferring sufficient kinetic energy to material atoms, only becomes significant when the ions have been sufficiently slowed down by electronic interactions. In the case of MeV light ions, this happens microns to millimeters below the surface. For material atoms displaced from this position, it is unlikely that there will be sufficient backwards momentum to reach the front-facing surface to remove atoms by sputtering. Measured sputtering yields for MeV protons at normal incidence on metals are as low as 10^{-5} atoms/ion, which would result in negligible mass loss from an interstellar spacecraft for total fluences in

the range of Equation 1 [39].

There may be sputtering from the sides of a relativistic spacecraft, since some portion of incident ions will effectively be grazing the surface, slowing down to speeds where the nuclear cross section is significant very close to perpendicular surfaces. To estimate the amount of grazing-incidence sputtering, consider the lateral distribution of implanted particles at relativistic speeds. The material and spacecraft velocity considered in this work that results in the largest lateral projected range is copper at 0.2c, for which the lateral range is about 30 μm , as determined by SRIM. As a first-order approximation, no hydrogen atom impacting further than 30 μm from the nearest perpendicular surface will reach that surface with enough energy to cause sputtering from it. Only approximately 40% of incident hydrogen meets this criterion, as illustrated in Figure 3.

Using Equation 2 to estimate the depth $\Delta x_{\text{erosion}}$ of eroded material:

$$\Delta x_{\text{erosion}} = \frac{\Phi Y(E, \theta)}{n} \quad (2)$$

from the fluence Φ , the sputtering yield $Y(E, \theta)$ for the ion-material pair, and the atomic density of the material n , the total effect of grazing-incidence sputtering can be estimated. Using the maximum sputtering yield of hydrogen on copper as a worst-case value, ~ 0.1 atoms per ion, the total depth of eroded material from grazing incidence sputtering will be no more than 4.7 °A per 1×10^{17} cm^{-2} total hydrogen fluence. Based on this analysis, erosion from light ion sputtering will be negligible, and the attention should be devoted to damage via gas accumulation.

2.2 Damage via Gas Accumulation

Implanted gas atoms in solids can drive damage through a number of distinct mechanisms: embrittlement, crack nucleation, swelling, bubble formation, blistering and flaking, exfoliation, and changes to macroscopic material parameters [44]. Which damage mechanism occurs depends on the implantation energy, angle, and fluence, the material's intrinsic strength and temperature during bombardment, and the chemical interactions of gas atoms with the material lattice [11]. At MeV energies and target temperatures well below melting, blistering is the most prevalent damage mechanism.

Blistering is a process through which gas atoms coalesce into bubbles, which grow and exert stress on the surrounding material [19]. If the internal bubble pressure reaches a critical value, inter-bubble cracking leads to the formation of large voids and deforms the surface nearest to the bubble layer [29][15]. Once a blister layer has formed, subsequent irradiation can result in significant, uncontrolled mass loss from that surface, through

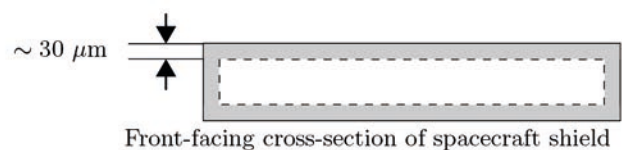
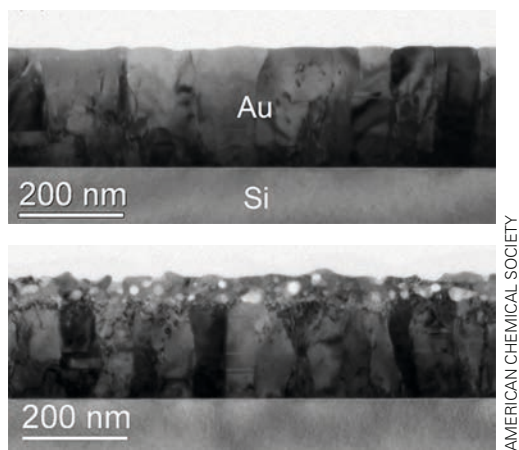


Fig.3 Illustration showing proportion of spacecraft front-facing cross section for which incident hydrogen and helium are within a suitable distance from a perpendicular surface to cause grazing-incidence sputtering.



AMERICAN CHEMICAL SOCIETY

Fig.4 (a) Gold sample before exposure. (b) Gold sample after exposure to $\Phi = 4 \times 10^{17} \text{ cm}^{-2}$ He ions at 4 keV. Blistering occurs at the depth of the projected range of He ions in the material. Reprinted with permission from [33].

repeated blister bursting and flaking of blister caps [47]. Blistering has been observed in spacecraft components [32] and in thin films tested for spaceflight [46]. An example of blistering by low energy helium bombardment is shown in Figure 4. At a fluence of $4 \times 10^{21} \text{ m}^{-2}$, blistering was observed; below this fluence, no blistering was found. At MeV energies, single large blisters have been observed that span the entire beam diameter [3]. If ISM exposure were to cause blistering on the front-facing shield of a gram-scale interstellar spacecraft, the potential for uncontrolled mass loss leading to non-correctable attitude deviations would result in direct irradiation of crucial spacecraft components and instruments and potential loss of communications.

At $0.05c$ – $0.2c$, hydrogen and helium will impact the front of the spacecraft with 1.176–19.36 MeV and 4.669–76.88 MeV respectively. At energies for which electronic interaction of hydrogen and helium in solids is dominated by Bethe-Bloch stopping (approximately 1 MeV/amu), helium implants with a depth distribution that lies within that of hydrogen, as seen in Figures 5 and 6. This leads to a mixed hydrogen-helium implanted layer that spans the entire front-facing cross section of the spacecraft at the depth of the ion range at that energy. In

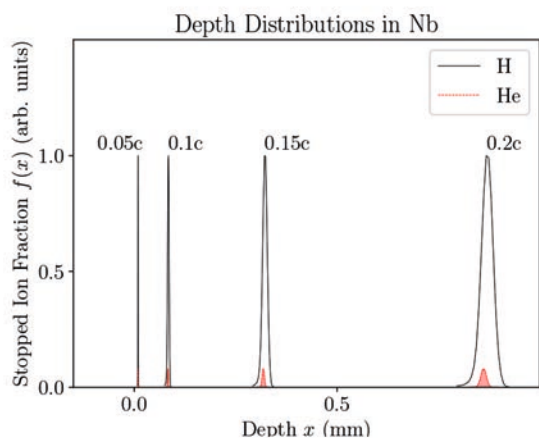


Fig.5 Hydrogen and helium implantation distributions in niobium at velocities from 0.05 – $0.2c$. The helium distributions (shaded) lie within the hydrogen distributions, leading to the mixed hydrogen-helium layer.

contrast to an ion beam target experiment, where blisters affect only a surface up to the size of the beam width the region effected by gas accumulation below the surface would span from one side of the shield to the other, causing lateral deformations and bulges on the sides of the spacecraft, with consequent formation of large blister caps and their removal via bursting or flaking, as shown in Fig. 7.

Co-implanted hydrogen and helium have a synergistic effect on gas accumulation-driven damage in metals and in semiconductor materials [20], [10], [1]. Determining the precise nature of the hydrogen-helium-material interaction is an ongoing effort, particularly in the research of potential PFCs for future fusion reactors [49], [9], [5] and in silicon, where co-implanted hydrogen and helium is used to exfoliate whole surface layers

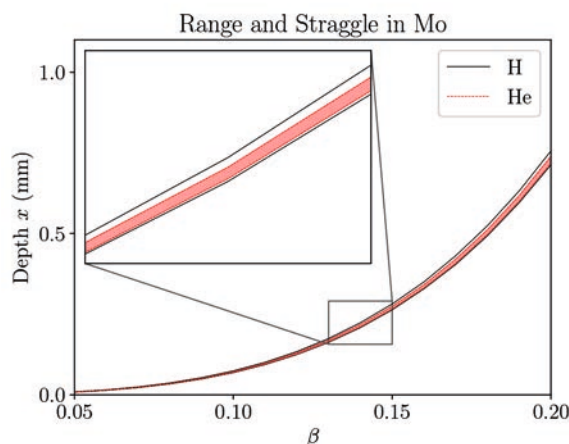


Fig.6 Range and straggle of hydrogen and helium in molybdenum at velocities from 0.05 – $0.2c$. The banded regions are centered on the range R_p and extend to $\pm\Delta R$. The helium distribution (shaded) lies within the hydrogen distribution. All materials simulated show the same general behavior, with differences in the magnitude of the range and straggle.

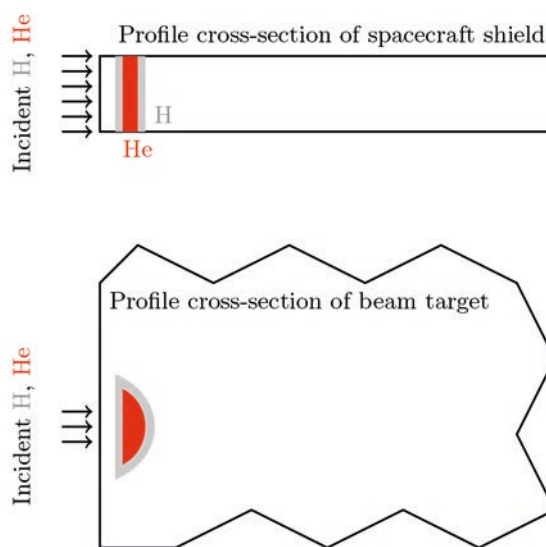


Fig.7 Illustrated comparison of implantation distributions for the case of wide-beam exposure (such as that experienced by a relativistic spacecraft traveling through the ISM) and for an ion beam target. In the spacecraft case, the gas accumulation layer spans the entire front-facing cross section.

as part of a process referred to as Smart-cut [8]. In metals, hydrogen is found to be trapped near helium bubbles [2], a potential mechanism for the observed lowering of the critical concentration of blistering for hydrogen and helium co-implantation [19], [29]. In silicon, the interaction of hydrogen and helium can reduce the critical fluence required for exfoliation by a factor of 2–3 compared to hydrogen or helium alone [31]. This interaction is greater than would be expected by the summation of the internal pressures of each species individually. Due to a lack of first-principles models and experimental results available in the literature on MeV-range hydrogen-helium co-implantation in metals, a quantitative estimate of this effect is difficult to make. For this study, a synergistic effect resulting in a critical fluence reduction factor of 2 is used, but further work is needed to determine the strength of this effect in potential shield material candidates.

To determine critical fluences for blistering on metal shields for interstellar spacecraft, the internal gas pressure model for homogeneous materials is used [29]. In its simplest form, the model estimates the local gas pressure in a solid, p_g , from the local gas concentration, c_g , and the energy of dissolution of that gas in the material, E_d , as seen in Equation 3. Dissolution energies for a number of pure metallic shield material candidates are shown in Table 1. Blistering occurs when the local gas pressure exceeds a critical value. Note that significant figures of the values listed in Table 1 are taken directly from the literature, but only 3 significant figures are propagated through calculations.

$$p_g = c_g E_d \tag{3}$$

An estimate of the local gas concentration can be found from the total fluence, or dose, of the gas incident on the target, Φ , and the standard deviation of the projected range of the gas atoms in the material at the irradiation energy ΔR , also known as the straggle, as shown in Equation 4. Straggle increases with incident energy, since energetic particles travel through more of the material before stopping and experience more collisions resulting in small-angle deviations. Higher speeds result in a higher critical fluence, because the wider implantation distribution lowers the average gas concentration in the material. Surface roughening or material preparation such as sintering will increase straggle in materials, leading to an increased critical fluence.

$$c_g = \frac{\Phi}{\Delta R} \tag{4}$$

In the original model, the yield strength, σ_y , was proposed as the critical pressure for inter-bubble cracking and blister formation. Critical fluence dependence on temperature does follow the dependence on temperature of the yield strength in many metals [19]. However, examination of empirical critical fluences performed at low energy (keV range) suggested that the critical pressure for blistering was instead best estimated by 0.1E, where E is the elastic modulus of the material [29]. At higher energy irradiations, however, this estimate no longer holds [16]. For 2.2 MeV proton irradiation of tungsten, the critical fluence for blister formation was $\leq 3 \times 10^{17} \text{ cm}^{-2}$, which is at least an order of magnitude below the critical fluence of keV-range irradiation [17]. This is a surprising result since the straggle at 2.2 MeV is an order of magnitude larger than that of 50 keV, so by Equation 3 and using the estimate of the critical pressure as 0.1E, the critical fluence should have been $\approx 2 \times 10^{19} \text{ cm}^{-2}$, two orders of magnitude higher. Segev et al. hypothesize

TABLE 1: Dissolution energies of hydrogen and helium in a selection of pure, homogeneous metallic shield candidates

Material	$E_{d,H}$ [eV]	$E_{d,He}$ [eV]
Cu	0.5032 ⁽¹⁾	0.891 ⁽²⁾
Al	0.71 ⁽³⁾	0.792 ⁽²⁾
Nb	-0.35 ⁽⁴⁾	0.280 ⁽²⁾
W	1.04 ⁽⁵⁾	7.83 ⁽⁶⁾
Be	1 ⁽⁷⁾	0.492 ⁽⁸⁾

Dissolution energies from Terreault et al. and Langley are back-calculated using the internal gas pressure model and Martynenko’s empirical estimate of 0.1E as the critical pressure for low-energy experiments, where E is the elastic modulus of the material. ⁽¹⁾[28] ⁽²⁾[48] ⁽³⁾[51] ⁽⁴⁾[35] ⁽⁵⁾[43] ⁽⁶⁾[21] ⁽⁷⁾[36] ⁽⁸⁾[26].

that the difference in critical fluence between keV- and MeV-range irradiations is due to gas atom escape to the surface, recombination of radiation induced defects with the surface, and significantly more sputtering at low energy.

Using the internal gas pressure model, Equations 3 and 4, the critical pressure for blistering for the experimental MeV irradiation was $\sim 480 \text{ MPa}$. This value is within about 10% of the yield strength, σ_y , of tungsten, suggesting that for MeV irradiation, a good estimate for the critical internal gas pressure for blistering is the yield strength. Thus, for the following analysis, the yield strength will be used as the critical pressure for blistering for metals exposed to MeV range light ion irradiation. Yield strengths and critical gas concentrations for candidate shield materials are shown in Table 2.

At low flux and long irradiation times, such as those experienced by a relativistic, interstellar spacecraft travelling through the ISM, diffusion may play a critical role in the development of gas accumulation damage. Diffusion coefficients of gas atoms in materials depend on the material temperature, the energetics of gas atoms in the material, the lattice structure of the material, and defects such as vacancies, interstitials, and grain boundaries. At MeV energies, significant damage is produced around the implantation distribution peaks of hydrogen and helium, which will limit diffusion. At concentrations above 0.1 ppm, helium tends to self-trap in metals, leading to helium clusters and eventually helium bubbles that are not mobile at low temperatures [50]. For an interstellar spacecraft with a copper shield traveling through the ISM with an average helium density of 0.03 cm^{-3} , 0.1 ppm helium concentration will be reached after travelling only $\sim 38 \text{ AU}$. Hydrogen is strongly trapped by helium clusters and bubbles, also reducing diffusion. Interstellar spacecraft trav-

TABLE 2: Yield strengths and critical local gas concentrations for blistering of pure metals from Equation 3 and Table 1*

Material	σ_y [MPa]	$c_{H,c} \text{ cm}^{-3}$	$c_{He,c} \text{ cm}^{-3}$
Al	20	1.76×10^{20}	1.58×10^{20}
Cu	33	4.09×10^{20}	2.31×10^{20}
Nb	414	n/a	9.21×10^{21}
W	550	3.30×10^{21}	4.38×10^{20}
Be	240	1.50×10^{21}	3.05×10^{21}

*Niobium, having a negative hydrogen dissolution energy, will not blister from hydrogen accumulation alone [42].

eling through ISM of densities below 1 cm^{-3} will maintain a temperature at or below room temperature, further reducing diffusion [22]. For this analysis, due to radiation-induced vacancy production around the ion implantation distribution, helium self-trapping and hydrogen trapping by helium clusters and bubbles, diffusion will be neglected.

3 RESULTS

3.1 Implantation distributions

To determine the straggle of hydrogen and helium ions at relativistic speeds in materials, the BCA code SRIM is used. Simulation runs were performed using the standard lookup values for material densities, binding energies, threshold energies, and bulk binding energies included in SRIM. 10,000 computational ions are used for estimating range and straggle, and 100,000 computational ions are used to produce implantation distributions such as Figure 5. At MeV energies, the straggle of helium in metals is smaller than that of hydrogen. Lighter elements scatter light ions more, leading to a correlation between atomic mass and straggle, as seen in Tables 3 and 5. Typically, at 0.05c hydrogen and helium straggle is on the order of $1,000 \text{ }^\circ\text{A}$, at 0.1c on the order of $1 \text{ }\mu\text{m}$, and at 0.2c on the order of $10 \text{ }\mu\text{m}$.

3.2 Critical Fluence for Blistering

Using dissolution energies for pure metals from Table 1 and straggle from Tables 3–5, neglecting diffusion, and using the yield strengths from Table 2 as the critical local gas pressure for blistering, critical fluences for blistering for a number of pure metallic candidate shield materials can be determined using Equation 3. For materials that readily dissolve hydrogen, such as niobium, no blistering is expected for hydrogen irradiation [42]. Critical fluences at 0.05, 0.1, and 0.2c are shown for copper, aluminum, niobium, and tungsten, four candidate metallic shield materials with different material properties, in Table 6. Shield materials that have low yield strength, such as copper and aluminum, have relatively low critical fluences despite the low dissolution energies for helium and the increased straggle in copper and aluminum. Niobium, with its relatively high yield strength, negative hydrogen dissolution energy, and relatively low helium dissolution energy, seems to be a particularly good choice for resisting blistering.

To estimate the effect of hydrogen-helium synergy in materials, critical hydrogen fluences for a simple summation of hydrogen and helium internal gas pressure are found, as shown in Equation 5, where x is the ratio of helium to hydrogen in the beam. Additionally presented are critical hydrogen fluences for hydrogen and helium with a synergistic fluence reduction factor of 2.

$$\Phi_c = \frac{\sigma_y}{\frac{E_{d,H}}{\Delta R_H} + x \frac{E_{d,He}}{\Delta R_{He}}} \quad (5)$$

4 DISCUSSION

4.1 Survivability of Metallic Shields

Survivability of simple metallic shields is investigated along line-of-sight paths to the stars in Table 9. Using the line-of-sight column density to each star as the total fluence for a journey to that star, and the critical fluence for blistering as the distance at which mission failure occurs, stars reachable with

TABLE 3: Straggle of hydrogen and helium at 0.05c from SRIM

Material	$\Delta RH(0.05c)$	$\Delta RHe(0.05c)$
Al	5040 $^\circ\text{A}$	3840 $^\circ\text{A}$
Cu	4090 $^\circ\text{A}$	2870 $^\circ\text{A}$
Nb	5210 $^\circ\text{A}$	2940 $^\circ\text{A}$
W	6140 $^\circ\text{A}$	3980 $^\circ\text{A}$
Be	4450 $^\circ\text{A}$	2890 $^\circ\text{A}$

TABLE 4: Straggle of hydrogen and helium at 0.1c from SRIM

Material	$\Delta RH(0.1c)$	$\Delta RHe(0.1c)$
Al	3.81 μm	2.29 μm
Cu	2.28 μm	1.05 μm
Nb	3.46 μm	1.76 μm
W	2.98 μm	1.46 μm
Be	3.56 μm	2.42 μm

TABLE 5: Straggle of hydrogen and helium at 0.2c from SRIM

Material	$\Delta RH(0.2c)$	$\Delta RHe(0.2c)$
Al	34.8 μm	19.0 μm
Cu	17.0 μm	8.35 μm
Nb	23.4 μm	10.4 μm
W	20.7 μm	9.82 μm
Be	35.9 μm	18.9 μm

TABLE 6: Critical fluences for hydrogen alone and helium alone at 0.05, 0.1, and 0.2c for several shield candidate metals

Material	β	$\Phi_{c,H} [\text{cm}^{-2}]$	$\Phi_{c,He} [\text{cm}^{-2}]$
Cu	0.05	1.67×10^{16}	6.64×10^{15}
	0.1	9.34×10^{16}	2.42×10^{16}
	0.2	6.96×10^{17}	1.93×10^{17}
Al	0.05	8.85×10^{15}	6.05×10^{15}
	0.1	6.69×10^{16}	3.60×10^{16}
	0.2	6.12×10^{17}	3.00×10^{17}
Nb	0.05	N/A	2.71×10^{17}
	0.1	N/A	1.62×10^{18}
	0.2	N/A	9.61×10^{18}
W	0.05	2.03×10^{17}	1.75×10^{16}
	0.1	9.83×10^{17}	6.39×10^{16}
	0.2	6.84×10^{18}	4.31×10^{17}
Be	0.05	6.76×10^{16}	4.33×10^{16}
	0.1	5.33×10^{17}	7.37×10^{17}
	0.2	5.38×10^{18}	5.76×10^{18}

each shield material are shown in Figure 8. Using an idealized, homogeneous model of the ISM composed of 0.3 cm^{-3} hydrogen and 0.03 cm^{-3} , critical distances for blistering for the shield material candidates are shown in Table 8. Tungsten shields will be susceptible to helium blistering, due to the high energy of dissolution of helium in tungsten, 7.83 eV. Niobium, due to its resistance to hydrogen blistering, is a promising shield material choice, although the synergistic effect with helium has not

been investigated experimentally at MeV energies. No other pure metallic shield material will resist blistering for a mission to a nearby star traveling 0.05c.

Experimental work on the effect of this hydrogen-helium synergy at MeV energies is needed to reach a definitive conclusion on the survivability of metallic shields on interstellar spacecraft. Without such experimental work, internal gas pressure models imply that metals that readily dissolve hydrogen are a good choice for interstellar spacecraft shielding. Traveling at 0.2c or faster spreads out the ISM implantation distribution enough that many shield materials become viable for journeys to several nearby stars. At slower speeds, many common metals will experience blistering or flaking, and the resulting uncontrolled mass loss may cause mission critical deviations in attitude, leading to loss of communications or damage to spacecraft components and instruments.

4.2 Mitigation Strategies

This analysis suggests a number of mitigation strategies to resist blistering of interstellar spacecraft shielding. First, manufacturing spacecraft shields from metals that readily dissolve hydrogen will limit the effect of blistering caused by ISM impacts. However, choice of shield material candidates must balance mass, cost of manufacture, and structural properties against radiation resistance. Alternative strategies to mitigate blistering and flaking may make lighter and cheaper materials more resistant to blistering.

One choice is to use a sintered metal material in the shield around the implantation distribution peak. Sintered aluminum exhibits a reduced blistering erosion rate by three orders of magnitude [41]. Sintered beryllium exhibited a blistering erosion yield reduced by one order of magnitude [12]. Additionally, microstructural effects on blistering in metals are significant; single crystal tungsten displays a marked resistance to hydrogen blistering at high energies, with a critical dose one order of magnitude greater than that of polycrystalline tungsten at target temperatures of 450–600 K and a factor of two larger at room temperature [17]. Using sintered materials or surface treatment is a cheap and effective mitigation strategy, although its effectiveness has not been experimentally investigated for MeV irradiation.

Spacecraft geometry plays a role in how much material is irradiated by travel through the ISM. An arrow or needle-like configuration will expose significantly less spacecraft volume to mixed hydrogen-helium-material conditions, and reduce the effect of blistering or flaking even if the critical fluence is reached [27].

Another option is to use metals with a low melting temperature, such as mercury, gallium, or lithium. Lithium in particular is a candidate for liquid-metal plasma-facing components in fusion reactors, because of its ability to readily absorb hydrogen and its low atomic number. At temperatures near the melting point, irradiation blistering at keV energies is reduced [19]. However, for tungsten irradiated with 2.2 MeV protons, the critical dose was temperature independent up to temperatures of 700 K [16]. More work on the effect of temperature on high-energy radiation blistering is needed to determine if this is an effective mitigation strategy.

Ceramics and porous materials offer a low-Z possibility for interstellar spacecraft shielding. At MeV energies, however,

TABLE 7: Critical hydrogen fluences for blistering for a beam of 10% helium*

Material	β	Φ_c [cm ⁻²]	$\Phi_c/2$
Cu	0.05	1.34×10 ¹⁶	6.68×10 ¹⁵
	0.1	6.74×10 ¹⁶	3.37×10 ¹⁶
	0.2	5.12×10 ¹⁷	2.56×10 ¹⁷
Al	0.05	7.72×10 ¹⁵	3.86×10 ¹⁵
	0.1	5.64×10 ¹⁶	2.82×10 ¹⁶
	0.2	5.08×10 ¹⁷	2.54×10 ¹⁷
Nb	0.05	2.71 ×10 ¹⁸	1.36×10 ¹⁸
	0.1	1.62×10 ¹⁹	8.08×10 ¹⁸
	0.2	9.61×10 ¹⁹	4.80×10 ¹⁹
W	0.05	9.38×10 ¹⁶	4.69×10 ¹⁶
	0.1	3.87×10 ¹⁷	1.94×10 ¹⁷
	0.2	2.64×10 ¹⁸	1.32×10 ¹⁸
Be	0.05	6.20×10 ¹⁶	3.10×10 ¹⁶
	0.1	4.97×10 ¹⁷	2.49×10 ¹⁷
	0.2	4.92×10 ¹⁸	2.46×10 ¹⁸

* for the summed gas pressure from Equation 5 and using a hydrogen-helium synergy critical fluence reduction factor of 2

TABLE 8: Distance in an idealized ISM consisting of 0.3 cm⁻³ hydrogen and 0.03 cm⁻³ helium at which blistering occurs for each ISM species and for a summed internal gas pressure of the two at travel speeds of 0.05, 0.1, and 0.2c

Material	β	$d_{c,H}$ [ly]	$d_{c,He}$ [ly]	$d_{c,H+He}$ [ly]
Cu	0.05	0.0589	0.234	0.0471
	0.1	0.329	0.853	0.238
	0.2	2.45	6.80	1.80
Al	0.05	0.0312	0.213	0.0272
	0.1	0.236	1.27	0.199
	0.2	2.16	10.6	1.79
Nb	0.05	N/A	9.56	9.56
	0.1	N/A	57.0	57.0
	0.2	N/A	338	338
W	0.05	0.714	0.615	0.330
	0.1	3.46	2.25	1.36
	0.2	24.1	15.2	9.31
Be	0.05	0.235	1.53	0.218
	0.1	1.88	26.0	1.75
	0.2	18.9	203	17.3

ceramic materials exhibit blistering and exfoliation at similar fluences to tungsten, with little dependence on atomic composition, due to the limited solubility of hydrogen and helium in these materials [55].

5 CONCLUSION

Damage to a relativistic spacecraft via ISM gas implantation is a potentially mission-threatening phenomenon. As has been shown, sufficient sub-surface implantation of hydrogen and helium in metallic materials leads to macroscopic damage includ-

ing bubble formation, swelling, blistering, and exfoliation. These effects can lead to trajectory alteration, loss of attitude control, or damage to the spacecraft bus itself. In order to mitigate these phenomena, various metallic materials were studied as candidates for a circumferential shield. It was found that hydrogen and helium implant in a thin enough layer to drive gas accumulation damage such as blistering. Accounting for the synergistic effect of hydrogen and helium in materials leads to reduced critical fluences for damage to occur. It was also found that, in general, the yield strength of the given shield material is an adequate approximation of the failure point with regards to inter-bubble fracture leading to macroscopic blistering. This can lead to exfoliation of surface layers, bubble bursting events, and morphological changes that pose a threat to interstellar missions.

It was found that the width of the gas implantation distribution depends strongly on the spacecraft β , or equivalently the incident particle energies. Since higher energy impacts result in deeper implantation depths, these particles must travel through more shield material before coming to a stop, and thus experience more small-angle scattering interactions, increasing the width of the implantation distribution. This reduces the local gas concentration around the average implantation depth, thus increasing the critical dose for the onset of damaging effects like blistering. As a result, it was found that the onset of blistering occurs later for faster travelling spacecraft. Thus, in general, faster spacecraft can withstand larger doses

of incoming ISM gas and can thus effectively travel further. This is shown in Figure 8, where it can be seen that for both tungsten and beryllium shields, more stars can be reached at $\beta = 0.2$ than at $\beta = 0.1$. Shield materials that can effectively dissolve hydrogen, such as niobium, are a promising choice for circumferential shielding of interstellar spacecraft. Mitigation strategies, such as surface modification and using sintered metal powders, offer 1-3 orders of magnitude reductions in critical fluences, allowing for the use of even poorly performing metallic shield materials, such as aluminum. Without any consideration or mitigation, gas accumulation poses a significant threat to gram-scale, relativistic spacecraft, especially at speeds below 0.2c. A Starshot-style mission will depend on a light sail for directed energy propulsion; however, our analysis on implanted particle effects does not extend to that of a solar sail which is thinner than the range of hydrogen and helium at relativistic speeds; for this case, an analysis of the transmission, forward and backward sputtering, reflection, and thermal spikes will need to be completed.

ACKNOWLEDGMENTS

Funding for this program comes from NASA grants NIAC Phase I DEEP-IN – 2015 NNX15AL91G and NASA NIAC Phase II DEIS – 2016 NNX16AL32G and the NASA California Space Grant NASA NNX10AT93H as well as a generous gift from the Emmett and Gladys W. fund.

APPENDIX

TABLE 9: Profiles of stars plotted in Figures 2 and 8*

	Name	Dist. (ly)	R.A. (deg)	Dec. (deg)	log10(NHI) (cm ⁻²)	Mass M _⊙	Radius R _⊙	Temp. (K)	Exoplanets (#)	Shield Material ($\beta = 0.2$)
1	α Cen A	4.40	219.9	-60.8	17.6	1.100	1.22	5790	1	Al, Cu, Be, W, Nb
2	α CMa B	8.48	101.3	-16.7	17.6	1.018	0.008	25,000	0	Al, Cu, Be, W, Nb
3	Eri	10.44	53.2	-9.5	17.8	0.820	0.735	5084	0	Cu, Be, W, Nb
4	61 Cyg A	11.35	316.7	38.7	17.8	0.700	0.665	4526	0	Cu, Be, W, Nb
5	α CMi	11.42	114.8	5.2	17.9	1.499	2.048	6530	0	Be, W, Nb
6	Ind	11.74	330.8	-56.8	18.0	0.754	0.732	4630	1	Be, W, Nb
7	α Ceti	11.74	26.0	-15.9	18.0	0.783	0.793	5344	≥ 1	Be, W, Nb
8	40 Eri A	16.31	63.8	-7.7	17.8	0.840	0.810	5300	1	Cu, Be, W, Nb
9	χ^1 Ori	28.38	88.6	20.3	17.8	0.979	1.081	5955	0	Be, W, Nb
10	δ Eri	29.35	55.8	-9.8	17.9	1.330	2.327	5055	0	Be, W, Nb
11	κ^1 Ceti	30.01	49.8	3.4	17.5	1.037	0.950	5708	0	Al, Cu, Be, W, Nb
12	β Gem	33.59	116.3	28.0	18.0	1.910	8.800	4666	1	Be, W, Nb
13	HR 857	33.92	53.2	-9.5	18.0	0.840	0.750	5225	0	Be, W, Nb
14	HR 1925	39.79	85.3	53.5	18.3	0.871	0.810	5257	0	Be, W, Nb
15	α Aur	42.07	79.2	46.0	18.2	2.569	11.980	4970	0	Be, W, Nb
16	HR 8	44.68	1.7	29.0	18.3	0.889	0.917	5509	0	Be, W, Nb
17	β Cas	54.47	2.3	59.1	18.2	1.910	3.43	7079	0	Be, W, Nb

* Suitable shield materials considered here are homogeneous, though it is likely that granular, powdered, or sintered materials will better resist damaging effects like blistering and thus can likely travel to farther targets. Shield material choice at 0.2c does not include hydrogen-helium synergistic effect

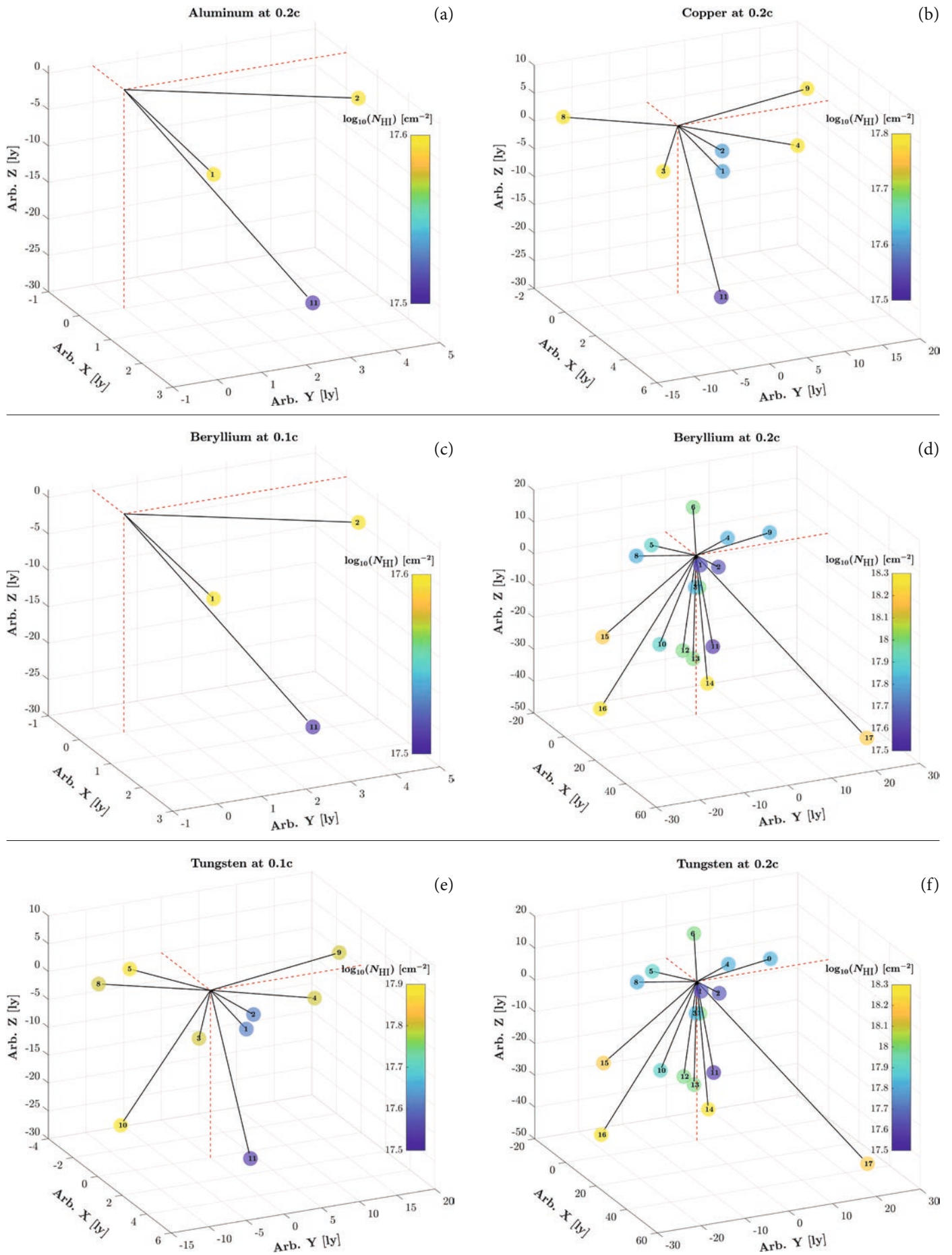


Fig.9 Stars from Fig. 2 for which the HI column density along the line-of-sight is less than the critical dose of the shield material. Materials and velocities shown are (a) aluminum at 0.2c, (b) copper at 0.2c, beryllium at (c) 0.1c and (d) 0.2c, and tungsten at (e) 0.1c and (f) 0.2c.

REFERENCES

1. P. Lubin, "A Roadmap to Interstellar Flight," *JBIS*, **69**, pp.40-72, 2016.
2. N. Kulkarni, P. Lubin, and Q. Zhang, "Relativistic Spacecraft Propelled by Directed Energy," *The Astronomical Journal*, **155**, p.155, 2018.
3. P. Srinivasan, G. B. Hughes, P. Lubin, Q. Zhang, J. Madajian, T. Brashears, N. Kulkarni, A. Cohen, and J. Griswold, "Stability of Laser-Propelled Wafer Satellites," in *Planetary Defense and Space Environment Applications*, **9981**, p.998105, 2016.
4. B. T. Draine, *Physics of the Interstellar and Intergalactic Medium*, Princeton University Press, Princeton and Oxford, 2010.
5. R. S. Klessen and S. C. Glover, "Physical Processes in the Interstellar Medium," in *Star Formation in Galaxy Evolution: Connecting Numerical Models to Reality: Saas-Fee Advanced Course 43*. Swiss Society for Astrophysics and Astronomy, 2015.
6. T. Hoang, A. Lazarian, B. Burkhart, and A. Loeb, "The Interaction of Relativistic Spacecrafts with the Interstellar Medium," *The Astrophysical Journal*, **837**, p.5, 2017.
7. G. Gloeckler and J. Geiss, "Composition of the Local Interstellar Medium as Diagnosed with Pickup Ions," *Advances in Space Research*, **34**, pp.53-60, 2004.
8. S. Redfield and J. L. Linsky, "The Structure of the Local Interstellar Medium. IV. Dynamics, Morphology, Physical Properties, and Implications of Cloud-Cloud Interactions," *The Astrophysical Journal*, **673**, pp.283-314, 2008.
9. S. Redfield, "Physical Properties of the Local Interstellar Medium," *Space Science Reviews*, **143**, no. 1-4, pp.323-331, 2009.
10. J. Biersack and L. Haggmark, "A Monte Carlo Computer Program for the Transport of Energetic Ions in Amorphous Targets," *Nuclear Instruments and Methods*, **174**, pp.257-269, 1980.
11. W. Eckstein, *Computer Simulation of Ion-Solid Interactions*, Springer-Verlag, Berlin, 1991.
12. M. T. Robinson, "The Binary Collision Approximation: Background and Introduction," *Radiation Effects and Defects in Solids*, **130-131**, pp.3-20, 1994.
13. J. F. Ziegler and J. P. Biersack, "The Stopping and Range of Ions in Matter," in *Treatise on Heavy-Ion Science*, pp.93-129, Springer US, Boston, 1985.
14. J. F. Ziegler, M. Ziegler, and J. Biersack, "SRIM - The Stopping And Range Of Ions In Matter," *Nuclear Instruments and Methods in Physics Research Section B: Beam Interactions with Materials and Atoms*, **268**, pp.1818-1823, 2010.
15. J. F. Ziegler, "Stopping of Energetic Light Ions in Elemental Matter," *Journal of Applied Physics*, **85**, pp.1249-1272, 1999.
16. H. Bolt, V. Barabash, W. Krauss, J. Linke, R. Neu, S. Suzuki, and N. Yoshida, "Materials for the Plasma-Facing Components of Fusion Reactors," in *Journal of Nuclear Materials*, **329-333**, pp.66-73, 2004.
17. R. A. Pitts, S. Carpentier, F. Escourbiac, T. Hirai, V. Komarov, A. S. Kukushkin, S. Lisgo, A. Loarte, M. Merola, R. Mitteau, A. R. Raffray, M. Shimada, and P. C. Stangeby, "Physics Basis And Design Of the ITER Plasma-Facing Components," in *Journal of Nuclear Materials*, **415**, pp.S947-S964, 2011.
18. D. Kato, H. Iwakiri, Y. Watanabe, K. Morishita, and T. Muroga, "Super-Saturated Hydrogen Effects on Radiation Damages in Tungsten under the High-Flux Divertor Plasma Irradiation," *Nuclear Fusion*, **55**, 2015.
19. N. Matsunami, Y. Yamamura, Y. Itikawa, N. Itoh, Y. Kazumata, S. Miyagawa, K. Morita, R. Shimizu, and H. Tawara, "Energy Dependence of the Ion-Induced Sputtering Yields of Monatomic Solids," *Atomic Data and Nuclear Data Tables*, **31**, pp.1-80, 1984.
20. J. Bohdanský, "A Universal Relation for the Sputtering Yield of Monatomic Solids at Normal Ion Incidence," *Nuclear Inst. and Methods in Physics Research B*, **2**, pp.587-591, 1984.
21. J. E. Robinson and D. A. Thompson, "Particle Emission from Metal Surfaces Irradiated with MeV Protons," *Physical Review Letters*, **33**, no. 26, pp.1569-1572, 1974.
22. B. M. U. Scherzer, "Development of Surface Topography Due to Gas Ion Implantation," pp.271-355, 1983.
23. S. K. Das and M. Kaminsky, "Radiation Blistering of Structural Materials for Fusion Devices and Reactors," *Journal of Nuclear Materials*, **53**, no. C, pp.115-122, 1974.
24. M. I. Guseva and Y. V. Martynenko, "Radiation Blistering," *Soviet Physics - Uspekhi*, **24**, pp.996-1007, 1981.
25. Y. V. Martynenko, "Damage to Materials in Radiation Blistering," *Soviet Journal of Plasma Physics*, **3**, no. 3, pp.395-397, 1977.
26. J. Evans, "A Mechanism of Surface Blistering on Metals Irradiated with Helium Ions," *Journal of Nuclear Materials*, **61**, pp.1-7, 1976.
27. B. Terreault, "When Are Blistering Or Flaking Repetitive?," *Journal of Nuclear Materials*, **93-94**, pp.707-712, 1980.
28. M. G. Pelizzo, A. J. Corso, P. Zuppella, D. L. Windt, G. Mattei, and P. Nicolosi, "Stability of Extreme Ultraviolet Multilayer Coatings to Low Energy Proton Bombardment," *Optics Express*, **19**, no. 16, pp.14838-14844, 2011.
29. M. Sznajder, U. Geppert, and M. R. Dudek, "Hydrogen Blistering under Extreme Radiation Conditions," *npj Materials Degradation*, **2**, p.3, 2018.
30. S. R. Bhattacharyya, T. K. Chini, D. Ghose, and D. Basu, "On the Formation of Exfoliation on the Reverse Unbombarded Face of a Tungsten Foil under MeV Alpha Particle Irradiation," *Nuclear Inst. and Methods in Physics Research B*, **53**, pp.355-357, 1991.
31. M. G. Pelizzo, A. J. Corso, E. Tassarolo, R. Böttger, R. Hübner, E. Napolitani, M. Bazzan, M. Rancan, L. Armelao, W. Jark, D. Eichert, and A. Martucci, "Morphological and Functional Modifications of Optical Thin Films for Space Applications Irradiated with Low-Energy Helium Ions," *ACS Applied Materials & Interfaces*, **10**, pp.34781-34791, 2018.
32. E. Hayward and C. Deo, "Synergistic Effects in Hydrogen-Helium Bubbles," *Journal of Physics: Condensed Matter*, **24**, p.265402, 2012.
33. J. Dai, Z. Xue, M. Zhang, X. Wei, G. Wang, and Z. Di, "Influence of Hydrogen Fluence on Surface Blistering of H and He Co-Implanted Ge," *Nuclear Instruments and Methods in Physics Research, Section B: Beam Interactions with Materials and Atoms*, **368**, pp.86-89, 2016.
34. A. Agarwal, T. E. Haynes, V. C. Venezia, O. W. Holland, and D. J. Eaglesham, "Efficient Production of Silicon-On-Insulator Films by Co-Implantation of He+ with H+," *Applied Physics Letters*, **72**, no. 9, pp.1086-1088, 1998.
35. M. Thompson, A. Deslandes, T. W. Morgan, R. G. Elliman, G. De Temmerman, P. Kluth, D. Riley, and C. S. Corr, "Observation of a Helium Ion Energy Threshold for Retention in Tungsten Exposed to Hydrogen/Helium Mixture Plasma," *Nuclear Fusion*, **56**, 2016.
36. R. A. Causey, D. F. Cowgill, R. Doerner, R. Kolasinski, B. Mills, D. Morse, J. Smugeresky, W. R. Wampler, R. Williams, and D. Huber, "Deuterium Retention in Tungsten at Elevated Temperatures," in *Journal of Nuclear Materials*, **415**, 2011.
37. S. Blondel, D. E. Bernholdt, K. D. Hammond, and B. D. Wirth, "Continuum-Scale Modeling of Helium Bubble Bursting under Plasma-Exposed Tungsten Surfaces," *Nuclear Fusion*, **58**, p.126034, 2018.
38. M. Bruel, "Separation of Silicon Wafers by the Smart-Cut Method," *Materials Research Innovations*, **3**, no. 1, pp.9-13, 1999.
39. Z. J. Bergstrom, M. A. Cusentino, and B. D. Wirth, "A Molecular Dynamics Study of Subsurface Hydrogen-Helium Bubbles in Tungsten," *Fusion Science and Technology*, **71**, pp.122-135, 2017.
40. O. Moutanabbir and B. Terreault, "Effects in Synergistic Blistering of Silicon by Co-implantation of H, D, And He Ions," *Applied Physics Letters*, **86**, pp.1-3, 2005.
41. H. Magnusson and K. Frisk, "Diffusion, Permeation and Solubility of Hydrogen in Copper," *Journal of Phase Equilibria and Diffusion*, **38**, pp.65-69, 2017.
42. B. Terreault, R. G. St-Jacques, G. Veilleux, J. G. Martel, J. L'Ecuyer, C. Brassard, and C. Cardinal, "Helium Irradiations Of Copper at 1 to 25 keV: Range Profiles, Reemission, and Blistering," *Canadian Journal of Physics*, **56**, pp.235-247, 1978.
43. C. Wolverton, V. Ozoliņš, and M. Asta, "Hydrogen in Aluminum: First-Principles Calculations of Structure and Thermodynamics," *Physical Review B - Condensed Matter and Materials Physics*, **69**, p.144109, 2004.
44. A. Pundt and R. Kirchheim, "Hydrogen in Metals: Microstructural Aspects," *Annual Review of Materials Research*, **36**, pp.555-608, 2006.
45. J. Roth and K. Schmid, "Hydrogen in Tungsten as Plasma-Facing Material," in *Physica Scripta T*, **T145**, p.014031, 2011.
46. K. O. Henriksson, K. Nordlund, J. Keinonen, D. Sundholm, and M. Patzschke, "Simulations of the Initial Stages of Blistering in Helium Implanted Tungsten," in *Physica Scripta T*, **T108**, pp.95-98, 2004.
47. C. Quirós, J. Mougnot, G. Lombardi, M. Redolfi, O. Brinza, Y. Charles, A. Michau, and K. Hassouni, "Blister Formation and Hydrogen Retention in Aluminium and Beryllium: A Modeling and Experimental Approach," *Nuclear Materials and Energy*, **12**, pp.1178-1183, 2017.
48. R. A. Langley, "Interaction of Implanted Deuterium and Helium

- with Beryllium: Radiation Enhanced Oxidation,” *Journal of Nuclear Materials*, **85-86**, pp.1123–1126, 1979.
49. I. Gavish Segev, E. Yahel, I. Silverman, and G. Makov, “Blister Formation at Subcritical Doses in Tungsten Irradiated by MeV Protons,” *Journal of Nuclear Materials*, **496**, pp.77–84, 2017.
50. I. Gavish Segev, E. Yahel, I. Silverman, A. Perry, L. Weismann, and G. Makov, “Hydrogen Blister Formation In Single Crystal and Polycrystalline Tungsten Irradiated by MeV Protons,” *Journal of Nuclear Materials*, **513**, pp.209–220, 2019.
51. J. Roth, R. Behrisch, and B. M. Scherzer, “Blistering of Niobium Due to 0.5 to 9 keV Helium and Hydrogen Bombardment,” *Journal of Nuclear Materials*, **53**, no. C, pp.147–153, 1974.
52. W. D. Wilson, C. L. Bisson, and M. I. Baskes, “Self-Trapping of Helium in Metals,” *Physical Review B*, **24**, no. 10, pp.5616–5624, 1981.
53. T. D. Rossing, S. K. Das, and M. Kaminsky, “Reduction of Surface Erosion in Fusion Reactors,” in *Journal of Vacuum Science and Technology*, **14**, pp.550–558, 1976.
54. S. K. Das and M. Kaminsky, “Reduction of Surface Erosion Caused by Helium Blistering in Sintered Beryllium and Sintered Aluminum Powder,” *Journal of Nuclear Materials*, **63**, pp.292–298, 1976.
55. S. J. Zinkle, “Effect of H and He Irradiation On Cavity Formation And Blistering In Ceramics,” in *Nuclear Instruments and Methods in Physics Research, Section B: Beam Interactions with Materials and Atoms*, **286**, pp.4–19, 2012.

Received 27 July 2020 Approved 2 November 2020